AIAA JOURNAL
Vol. 30, No. 3, March 1992

Aerodynamic Design Optimization Using Sensitivity Analysis and Computational Fluid Dynamics

Oktay Baysal* and Mohamed E. Eleshaky†
Old Dominion University, Norfolk, Virginia 23529

A new and efficient method is presented for aerodynamic design optimization, which is based on a computational fluid dynamics (CFD)-sensitivity analysis algorithm. The method is applied to design a simplified scramjet-afterbody configuration for an optimized axial thrust. The Euler equations are solved for the inviscid analysis of the flow, which provides the objective function and the constraints of the optimization problem. The CFD analysis is then coupled with the optimization procedure that used a constrained minimization method. The sensitivity coefficients, i.e., gradients of the objective function and the constraints, needed for the optimization are obtained using a quasi-analytical method rather than the traditional finite difference approximations. During the one-dimensional search of the optimization procedure, an approximate flow analysis (predicted flow) based on a first-order Taylor series expansion is used to reduce the computational cost. Finally, the sensitivity of the optimum objective function to various flowfield problem parameters, such as the Mach number, which are kept constant during the optimization, is computed to predict new optimum solutions. The flow analysis of the demonstrative example are compared with the experimental data. It is shown that the method is more efficient than the traditional methods.

Statement of the Problem

A TYPICAL constrained minimization or maximization problem entails a group of physical quantities that are used as design variables and another group of constant quantities called the problem parameters. In aerodynamic applications, the design variables and the problem parameters are either a geometric type or a flowfield type. Usually, the problem parameters are defined as those variables that are adequate to characterize the possible candidate design or operating conditions of the problem in question and their values are fixed and controlled by external factors. After obtaining the optimum design, it is of interest to know how the solution changes as problem parameters vary. Mathematically, this requires determining the derivatives of the objective function and the design variables with respect to those problem parameters of interest. These derivatives are called the sensitivity derivatives. This area of study, which is referred to as the sensitivity analysis, has been an active area of optimization research over the past decade.

In most optimization procedures, a dominant contributor to the computational cost is the calculation of the derivatives of the objective function and the constraints with respect to the design variables. These derivatives are called the sensitivity coefficients. Therefore, it is desirable in any optimization procedure to have efficient numerical or analytical methods to determine the sensitivity coefficients and efficient computational methods to solve the resulting equations. Generating the sensitivity coefficients by a finite difference approximation requires repeating the flowfield analysis with incremental values of the design variables. This approach has the disadvantage of being potentially computer intensive, especially if the governing equations are expensive to solve. A preferable approach is to obtain the sensitivity coefficients analytically from an appropriate set of discretized partial differential equations to eliminate these costly and repetitive analyses.[1,2]

To optimize a nozzle, a family of wall shapes needs to be determined which yields the maximum thrust. The calculus of variations combined with the method of characteristics has traditionally been used to provide such solutions. For example, the method of Rao[3] is used to design axially symmetric rocket nozzles, which is also adopted by Nickerson et al.[4] for the planar flow problems. Another approach is to limit the optimum nozzle contour to a specific class of surfaces described by free parameters. For example, an optimum nozzle contour may be sought among all the skewed parabolas passing through a fixed end point and tangent to a circular-arc initial expansion contour.[5]

The present aerodynamic design optimization method is demonstrated on a scramjet-afterbody configuration (Fig. 1) for maximum axial thrust. However, the purpose of this study is not finding an optimized scramjet-afterbody configuration of common interest. Therefore, this demonstrative example is sufficiently simplified by assuming the nozzle-afterbody contours to be planar surfaces (or lines in the 2-D case) with arbitrary inclinations (Fig. 2). It should be realized, however, that the aerodynamic design optimization method developed herein can be applied to any contour shape, if its local coordinates are defined as the geometric design variables.

Although the flowfield solutions for the simplified nozzle-afterbody configuration have been previously obtained[6] by solving the full Navier-Stokes equations, in the present investigation the two-dimensional, compressible, unsteady Euler equations are solved to determine the flowfield solution, and thereby the objective function and the constraints are evaluated. The primary reason for solving the Euler equations instead of the Navier-Stokes equations is that the derivation of the sensitivity equation is significantly simplified by excluding the viscous terms. A secondary reason is that the thrust values obtained from either set of the governing equations are not significantly different.[6]

Finally, the constrained minimization method of Vanderplaats[7] is used in the optimization procedure. The sensitivity analysis algorithm,[1] which is based on a first-order discretized form of the steady Euler equations, is used to calculate the sensitivity coefficients. Therefore, the present design method couples an inviscid CFD analysis with both a sensitivity analysis algorithm and an automated optimization procedure.

Presented as Paper 91-0471 at the AIAA 29th Aerospace Sciences Meeting, Reno, NV, Jan. 8–12, 1991; received Feb. 4, 1991; revision received June 17, 1991; accepted for publication June 20, 1991.

*Associate Professor, Mechanical Engineering and Mechanics Department. Senior Member AIAA.

†Graduate Research Assistant, Mechanical Engineering and Mechanics Department.

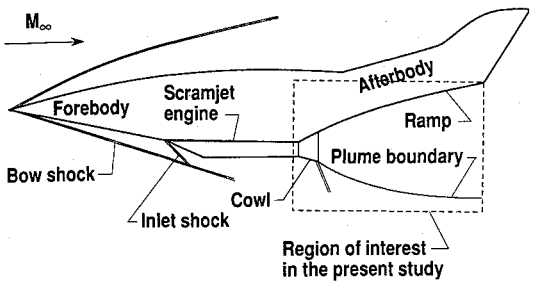

Fig. 1 Flowfield about a generic hypersonic vehicle.

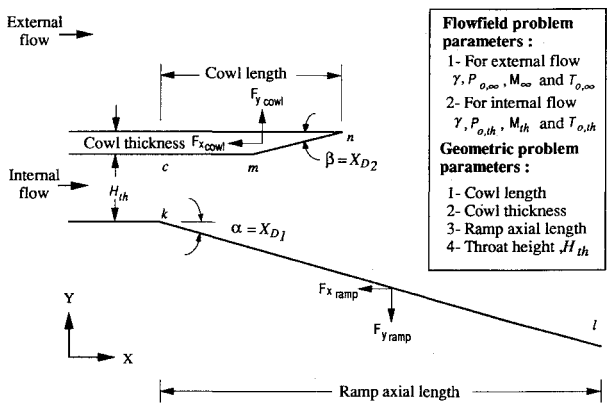

Fig. 2 Definition of the design variables, problem parameters, and the thrust force of the optimization problem.

Formulation of Optimization Problem

In the present demonstrative optimization problem, it is desired to determine the angles of the nozzle ramp α, and of the cowl β, that yield a maximum axial thrust force coefficient F, subject to constraints G_j, while keeping both types of problem parameters constant. Hence, in the present study, there are only two design variables $\bar{X}_D$, which are of the geometric type; namely, the angles α and β. There are seven flowfield problem parameters considered in this study; namely, the specific heat ratio γ, Mach numbers, total temperatures, and total pressures of both the external flow and the internal flow leading to the nozzle jet. Whereas, there are four geometric problem parameters, which are the throat height H_{th}, the cowl thickness, the cowl length, and the nozzle axial length (Fig. 2).

Mathematically, it is required to get

$$\max F(\bar{Q}(\bar{X}_D), \bar{X}_D) \tag{1}$$

subject to

$$G_j(\bar{Q}(\bar{X}_D), \bar{X}_D) \leq 0; \qquad j = 1, \text{NCON} \tag{2}$$

$$\bar{X}_{D\text{lower}} \leq \bar{X}_D \leq \bar{X}_{D\text{upper}} \tag{3}$$

where F is the objective function, NCON is the number of constraints, and $\bar{Q}$ is the vector of the conserved variables of the fluid flow. $\bar{X}_{D\text{lower}}$ and $\bar{X}_{D\text{upper}}$ are the lower and the upper bounds of the design variables. A judicious choice of the upper and lower bounds for the geometric design variables accelerates convergence of the optimum solution.

The axial component of the thrust force due to nozzle wall shape F_{axial}, is obtained by integrating numerically the pressure over the ramp and cowl surfaces.

$$F_{\text{axial}} = \int_k^l P_{\text{ramp}}\, dy + \int_m^n P_{\text{cowl}}\, dy \tag{4}$$

This force is normalized by the force associated with the inflow given by

$$F_{\text{inflow}} = \int_k^c P_{th}(1 + \gamma M_{th}^2)\, dy \tag{5}$$

In the case of an inflow parallel to the cowl with a constant Mach number, this force is centered at the midpoint of the line segment $\overline{kc}$, and its value is

$$F_{\text{inflow}} = P_{th}(1 + \gamma M_{th}^2)\, H_{th} \tag{6}$$

By definition, the axial thrust force coefficient is given by

$$F = \frac{F_{\text{axial}}}{F_{\text{inflow}}} \tag{7}$$

The axial thrust force coefficient is subject to three constraints (i.e., NCON = 3). First, the static pressure at the ramp tip P_l, is forced to reach a percentage C_1, of the freestream static pressure P_∞, such that a maximum expansion is reached without any back flow, i.e.,

$$G_1(\bar{X}_D) = 1 - \frac{P_l}{C_1 P_\infty} \leq 0 \tag{8}$$

The other two constraints are due to the static pressure at the cowl tip P_n, being forced to fall within specified limits (C_2 and C_3) of the freestream static pressure P_∞, such that a maximum expansion is reached without any back flow on either of the cowl surfaces, i.e.,

$$G_2(\bar{X}_D) = 1 - \frac{P_n}{C_2 P_\infty} \leq 0 \tag{9}$$

$$G_3(\bar{X}_D) = \frac{P_n}{C_3 P_\infty} - 1 \leq 0 \tag{10}$$

Sensitivity Coefficients

The derivatives of the objective function F, and constraints G_j, with respect to the design variables $\bar{X}_D$, are given by

$$\nabla F \equiv \frac{dF}{d\bar{X}_D} = \frac{\partial F}{\partial \bar{X}_D} + \left(\frac{\partial F}{\partial \bar{Q}}\right)^T \frac{\partial \bar{Q}}{\partial \bar{X}_D} \tag{11}$$

$$\nabla G_j \equiv \frac{dG_j}{d\bar{X}_D} = \frac{\partial G_j}{\partial \bar{X}_D} + \left(\frac{\partial G_j}{\partial \bar{Q}}\right)^T \frac{\partial \bar{Q}}{\partial \bar{X}_D}$$

$$j = 1, \text{NCON} \tag{12}$$

Different approaches for obtaining these derivatives are documented in Ref. 1. These are the traditional finite difference approach and the quasi-analytical or sensitivity analysis approach. In the quasi-analytical approach, two different methods are available; these are the direct method and the adjoint variable method. The choice of the particular sensitivity analysis method depends on the number of design variables (NDV) and adjoint vectors (NCON + 1). It is reported in Ref. 1, that if the number of design variables is less than the number of adjoint vectors, the direct method is more efficient than the adjoint variable method. Since in the present study, the number of design variables (NDV = 2) is less than the number of adjoint vectors (NCON + 1 = 4), the direct method is selected to determine the sensitivity coefficients.

Direct Method

The governing equations for two-dimensional, steady, compressible, inviscid flow of an ideal gas with constant specific heat ratio written in the residual vector form are

$$\bar{R}(\bar{Q}(\bar{X}_D), \bar{X}_D) = \frac{\partial \hat{f}}{\partial \xi} + \frac{\partial \hat{g}}{\partial \eta} = 0 \tag{13}$$

where $\hat{f}$ and $\hat{g}$ are the flux vectors in generalized coordinates (ξ, η) as given in Ref. 8.

The quasi-analytical approach[1] begins with the differentiation of Eq. (13) with respect to the design variables to yield the sensitivity equation:

$$\left[\frac{\partial \bar{R}}{\partial \bar{Q}}\right]\left\{\frac{\partial \bar{Q}}{\partial \bar{X}_D}\right\} = -\left[\frac{\partial \bar{R}}{\partial \bar{X}_D}\right] \tag{14}$$

Then Eq. (14) is solved for $\{\partial \bar{Q}/\partial \bar{X}_D\}$. It should be noted that Eq. (14) needs to be solved for each design variable X_D; however, the coefficient matrix $[\partial \bar{R}/\partial \bar{Q}]$ needs to be factorized once and for all. The remaining partial derivatives in Eqs. (11) and (12) can be evaluated analytically using Eqs. (7–10). The final step is determining the values of ∇F and ∇G_j.

Approximate Flow Analysis

In order to reduce the number of CFD analyses during the optimization process, an approximate flow analysis is suggested in Refs. 1 and 9, which is based on a Taylor-series expansion of the vector of conserved variables $\bar{Q}(\bar{X}_D^* + \Delta \bar{X}_D)$ about $\bar{X}_D^*$ as follows:

$$\bar{Q}(\bar{X}_D^* + \Delta \bar{X}_D) = \bar{Q}(\bar{X}_D^*) + \left(\frac{\partial \bar{Q}}{\partial \bar{X}_D}\right)_{X_D = X^*_D} \Delta \bar{X}_D + \cdots \tag{15}$$

Substituting Eq. (14) into Eq. (15) results in

$$\left[\frac{\partial \bar{R}(\bar{Q}(\bar{X}_D^*), \bar{X}_D^*)}{\partial \bar{Q}}\right]\Delta \bar{Q} = -\left[\frac{\partial \bar{R}(\bar{Q}(\bar{X}_D^*), \bar{X}_D^*)}{\partial \bar{X}_D}\right]\Delta \bar{X}_D \tag{16}$$

where $\Delta \bar{Q} = \bar{Q}(\bar{X}_D^* + \Delta \bar{X}_D) - \bar{Q}(\bar{X}_D^*)$.

Equation (16) gives the changes in $\bar{Q}$ due to the changes in $\bar{X}_D$. In other words, given the flowfield solution, $\bar{Q}(\bar{X}_D^*)$, associated with a configuration, $\bar{X}_D^*$, the flowfield solution, $\bar{Q}(\bar{X}^* + \Delta \bar{X}_D)$, associated with the configuration, $(\bar{X}_D^* + \Delta \bar{X}_D)$, is obtained via Eq. (16).

Although the approximate analysis is less accurate than the actual analysis, it is less costly in terms of computer time, especially when the number of flowfield governing equations is large, However, it is reported in Ref. 1 that the approximate analysis may be of acceptable accuracy up to $\pm 5\%$ changes in the design variables.

Sensitivity Solution Method

Equation (13) is solved by a first-order-accurate, implicit, upwind finite volume scheme.[8] An upwind discretized from of Eq. (13) at an interior cell (i, j) is as follows:

$$\begin{aligned}\bar{R}_{i,j} &= \hat{f}^+(\bar{Q}^-_{i+1/2,j}, M_{i+1/2,j}) - \hat{f}^+(\bar{Q}^-_{i-1/2,j}, M_{i-1/2,j}) \\ &+ \hat{f}^-(\bar{Q}^+_{i+1/2,j}, M_{i+1/2,j}) - \hat{f}^-(\bar{Q}^+_{i-1/2,j}, M_{i-1/2,j}) \\ &+ \hat{g}^+(\bar{Q}^-_{i,j+1/2}, M_{i,j+1/2}) - \hat{g}^+(\bar{Q}^-_{i,j-1/2}, M_{i,j-1/2}) \\ &+ \hat{g}^-(\bar{Q}^+_{i,j+1/2}, M_{i,j+1/2}) - \hat{g}^-(\bar{Q}^+_{i,j-1/2}, M_{i,j-1/2})\end{aligned} \tag{17}$$

where $\hat{f}^+, \hat{f}^-, \hat{g}^+$, and $\hat{g}^-$ are the operator-split inviscid fluxes.

As it is seen from Eq. (17), $\bar{R}_{i,j}$ is functionally dependent on the cell-face values of the conserved variables $(\bar{Q}^{\pm}_{i\pm 1/2, j\pm 1/2})$ and is also dependent on the geometric terms $(M_{i\pm 1/2, j\pm 1/2})$, which are involved in the transformation to the generalized coordinates and are evaluated at the cell-interface locations. Hence, the linear vector form of the left-hand side of Eq. (14) for an interior cell (i, j) can be written as

$$\begin{aligned}&[LHS \text{ of Eq. } (17)]_{i,j} \\ &= \frac{\partial \bar{R}_{i,j}}{\partial \bar{Q}^-_{i+1/2,j}}\frac{\partial \bar{Q}^-_{i+1/2,j}}{\partial \bar{X}_D} + \frac{\partial \bar{R}_{i,j}}{\partial \bar{Q}^-_{i-1/2,j}}\frac{\partial \bar{Q}^-_{i-1/2,j}}{\partial \bar{X}_D} \\ &+ \frac{\partial \bar{R}_{i,j}}{\partial \bar{Q}^+_{i+1/2,j}}\frac{\partial \bar{Q}^+_{i+1/2,j}}{\partial \bar{X}_D} + \frac{\partial \bar{R}_{i,j}}{\partial \bar{Q}^+_{i-1/2,j}}\frac{\partial \bar{Q}^+_{i-1/2,j}}{\partial \bar{X}_D} \\ &+ \frac{\partial \bar{R}_{i,j}}{\partial \bar{Q}^-_{i,j+1/2}}\frac{\partial \bar{Q}^-_{i,j+1/2}}{\partial \bar{X}_D} + \frac{\partial \bar{R}_{i,j}}{\partial \bar{Q}^-_{i,j-1/2}}\frac{\partial \bar{Q}^-_{i,j-1/2}}{\partial \bar{X}_D} \\ &+ \frac{\partial \bar{R}_{i,j}}{\partial \bar{Q}^+_{i,j+1/2}}\frac{\partial \bar{Q}^+_{i,j+1/2}}{\partial \bar{X}_D} + \frac{\partial \bar{R}_{i,j}}{\partial \bar{Q}^+_{i,j-1/2}}\frac{\partial \bar{Q}^+_{i,j-1/2}}{\partial \bar{X}_D}\end{aligned} \tag{18}$$

Each one of the $[\partial \bar{R}_{i,j}/\partial \bar{Q}^{\pm}_{i\pm 1/2, j\pm 1/2}]$ terms in Eq. (18) is obtained by differentiating the upwind discretized form given by Eq. (17) with respect to $(\bar{Q}^{\pm}_{i\pm 1/2, j\pm 1/2})$. For example, the term $[\partial \bar{R}_{ij}/\partial \bar{Q}^-_{i+1/2,j}]$ has the form

$$\frac{\partial \bar{R}_{i,j}}{\partial \bar{Q}^-_{i+1/2,j}} = \frac{\partial \hat{f}^+(\bar{Q}^-_{i+1/2,j}, M_{i+1/2,j})}{\partial \bar{Q}^-_{i+1/2,j}} \tag{19}$$

which is equivalent to the Jacobian matrix of $\hat{f}^+$. Therefore, denoting the Jacobian matrices of the split fluxes $\hat{f}^{\pm}$ and $\hat{g}^{\pm}$ by $A^{\pm}$ and $B^{\pm}$, respectively, Eq. (18) can be rewritten as

$$\begin{aligned}&[LHS \text{ of Eq. } (17)]_{i,j} \\ &= A^+_{i,j}\frac{\partial \bar{Q}^-_{i+1/2,j}}{\partial \bar{X}_D} - A^+_{i-1,j}\frac{\partial \bar{Q}^-_{i-1/2,j}}{\partial \bar{X}_D} \\ &+ A^-_{i+1,j}\frac{\partial \bar{Q}^+_{i+1/2,j}}{\partial \bar{X}_D} - A^-_{i,j}\frac{\partial \bar{Q}^+_{i-1/2,j}}{\partial \bar{X}_D} \\ &+ B^+_{i,j}\frac{\partial \bar{Q}^-_{i,j+1/2}}{\partial \bar{X}_D} - B^+_{i,j-1}\frac{\partial \bar{Q}^-_{i,j-1/2}}{\partial \bar{X}_D} \\ &+ B^-_{i,j+1}\frac{\partial \bar{Q}^+_{i,j+1/2}}{\partial \bar{X}_D} - B^-_{i,j}\frac{\partial \bar{Q}^+_{i,j-1/2}}{\partial \bar{X}_D}\end{aligned} \tag{20}$$

For the first-order-accurate upwind scheme, for example, the cell-face values of the conserved variables $(\bar{Q}^{\pm}_{i+1/2,j})$ and $(\bar{Q}^{\pm}_{i,j+1/2})$ are given by

$$\begin{aligned}\bar{Q}^-_{i+1/2,j} &= \bar{Q}_{i,j}, \qquad \bar{Q}^+_{i+1/2,j} = \bar{Q}_{i+1,j} \\ \bar{Q}^-_{i,j+1/2} &= \bar{Q}_{i,j}, \qquad \bar{Q}^+_{i,j+1/2} = \bar{Q}_{i,j+1}\end{aligned} \tag{21}$$

Hence, the values of the conserved variables at the cell-interface locations $(\bar{Q}^{\pm}_{i\pm 1/2, j\pm 1/2})$ can be viewed as functions of the values of the conserved variables of the neighboring cells evaluated at the centers. Therefore, the terms $[\partial \bar{Q}^{\pm}_{i\pm 1/2,j}/\partial \bar{X}_D]$ and $[\partial \bar{Q}^{+}_{i,j\pm 1/2}/\partial \bar{X}_D]$ in Eq. (20) can be expressed in terms of $[\partial \bar{Q}_{i\pm 1,j}/\partial \bar{X}_D]$, $[\partial \bar{Q}_{i,j}/\partial \bar{X}_D]$ and $[\partial \bar{Q}_{i,j\pm 1}/\partial \bar{X}_D]$. Hence, Eq. (20) is rewritten as

$$\begin{aligned}&[LHS \text{ of Eq. } (17)]_{i,j} = A^+_{i-1,j}\frac{\partial \bar{Q}_{i-1,j}}{\partial \bar{X}_D} \\ &+ \left(A^+_{i,j} + B^+_{i,j} + A^-_{i,j} + B^-_{i,j}\right)\frac{\partial \bar{Q}_{i,j}}{\partial \bar{X}_D} \\ &+ A^-_{i+1,j}\frac{\partial \bar{Q}_{i+1,j}}{\partial \bar{X}_D} + B^+_{i,j-1}\frac{\partial \bar{Q}_{i,j-1}}{\partial \bar{X}_D} \\ &+ B^-_{i,j+1}\frac{\partial \bar{Q}_{i,j+1}}{\partial \bar{X}_D}\end{aligned} \tag{22}$$

The Jacobian matrices $A^{\pm}$ and $B^{\pm}$ are usually available for interior cells from the flowfield solver. Hence, only a few computations are needed to assemble the coefficient matrix $[\partial\bar{R}/\partial\bar{Q}]$ in Eq. (14), if implicit treatment of the boundary conditions is used in the CFD algorithm. If not, then it is necessary to revise the residual expression (Eq. 17) at the boundary points to include the boundary conditions first and then assemble the coefficient matrix.

The coefficient matrix $[\partial\bar{R}/\partial\bar{Q}]$ is a square matrix with a block-banded structure, wherein all the nonzero elements are confined within a band formed by diagonals parallel to the main diagonal. It has the dimensions $(n \times n)$. For a two-dimensional computational domain with I cells in the ξ direction and J cells in the η direction, the matrix dimension, n, is (4IJ). The first-order upwind discretization of the governing equations yields a coefficient matrix with a subdiagonal bandwidth of (4J + 3) or (4I + 3), depending on the way the unknowns are ordered. Also, it results only in five nonzero diagonals in which the elements are (4 × 4) blocks. The unknown ordering reported in Ref. 1 is used in the present study to reduce the computer memory requirement.

Because of the function dependence of $(\bar{R}_{i,j})$ on $(M_{i\pm 1/2,j\pm 1/2})$, the right-hand side of Eq. (14) for an interior cell (i, j) can be written with the help of Eq. (17) as follows:

$$\frac{\partial\bar{R}_{i,j}}{\partial\bar{X}_D} = \left[\frac{\partial\hat{f}^+(\bar{Q}^-_{i+1/2,j},\, M_{i+1/2,j})}{\partial(M_{i+1/2,j})} + \frac{\partial\hat{f}^-(\bar{Q}^+_{i+1/2,j},\, M_{i+1/2,j})}{\partial(M_{i+1/2,j})}\right]\frac{\partial(M_{i+1/2,j})}{\partial\bar{X}_D} - \left[\frac{\partial\hat{f}^+(\bar{Q}^-_{i-1/2,j},\, M_{i-1/2,j})}{\partial(M_{i-1/2,j})} + \frac{\partial\hat{f}^-(\bar{Q}^+_{i-1/2,j},\, M_{i-1/2,j})}{\partial(M_{i-1/2,j})}\right]\frac{\partial(M_{i-1/2,j})}{\partial\bar{X}_D} + \left[\frac{\partial\hat{g}^+(\bar{Q}^-_{i,j+1/2},\, M_{i,j+1/2})}{\partial(M_{i,j+1/2})} + \frac{\partial\hat{g}^-(\bar{Q}^+_{i,j+1/2},\, M_{i,j+1/2})}{\partial(M_{i,j+1/2})}\right]\frac{\partial(M_{i,j-1/2})}{\partial\bar{X}_D} - \left[\frac{\partial\hat{g}^+(\bar{Q}^-_{i,j-1/2},\, M_{i,j-1/2})}{\partial(M_{i,j-1/2})} + \frac{\partial\hat{g}^-(\bar{Q}^+_{i,j-1/2},\, M_{i,j-1/2})}{\partial(M_{i,j-1/2})}\right]\frac{\partial(M_{i,j-1/2})}{\partial\bar{X}_D} \tag{23}$$

Determining the derivatives of the geometric terms $M_{i\pm 1/2,j\pm 1/2}$ with respect to the design variables $\bar{X}_D$, depends on whether analytical expression for $M = M(\bar{X}_D)$ exists or not. If this expression exists, then this differentiation is straightforward. Otherwise, a finite difference approximation for $\partial(M_{i\pm 1/2,j\pm 1/2})/\partial\bar{X}_D$ with a small step size $\Delta\bar{X}_D$ can be used.

Finally, the solution of the system of linear algebraic equations (14) is achieved by using a banded matrix solver.[10] This solver stores only the elements within the bandwidth of the matrix to economize on the computer memory. Then, the matrix is inverted by the Gauss elimination method. It has been previously shown in Ref. 1 that the banded matrix solver is more economical in solving the present system of linear equations than other available direct methods, such as a sparse matrix solver.

Design Algorithm

The overall process of aerodynamic design optimization consists of the CFD analysis, the approximate flow analysis, the optimization method, and pre- and post-optimization sensitivity analyses.

CFD Analysis

The flowfield simulations are performed using the general-purpose, finite volume Euler/Navier-Stokes CFD code VUMXZ3. This code has been applied to analyze a variety of complex internal and external flows.[11] It produces consistent and repeatable flow simulations in the sense that small perturbations to design variables are accurately reflected in the flowfield solution.

Preoptimization Sensitivity Analysis

A key part of the present design procedure is the sensitivity analysis, where the derivatives of the constraints, the objective function, and the conserved flow variables, with respect to the design variables, are computed. The derivatives quantify the effects of each design variable on the design and thereby identify the most important design changes to make en route to the optimum design.

Approximate Flow Analysis

Since the optimization process requires many evaluations of the objective function and constraints before an optimum design is obtained, the process can be very expensive if a CFD analysis is performed for each evaluation. However, it is pointed out in Refs. 7 and 9 that the optimization process primarily uses analysis results to move in the direction of the optimum design (i.e., one-dimensional search direction). Hence, an analysis needs to be made only occasionally during the design process and always at the end to check the final design. In the present study, approximate flow analyses using Eq. (16) are performed through the one-dimensional search of the optimization process, whereas the CFD analysis is performed only when new gradients of constraints and objective function are needed, i.e., when the search direction changes.

Optimization Algorithm

The present nonlinear, constrained optimization problem is solved using the modified feasible directions method developed by Vanderplaats[7] and implemented in the general-purpose optimization program ADS.[12] The procedure starts by initializing the values of the design variables (i.e., an initial computational grid). Then, a CFD analysis is performed to obtain the flowfield solution based on these initial values of the design variables. Next, the sensitivity analysis is performed to obtain the gradients of both the objective and the constraints for these initial values of design variables and their corresponding flowfield solution. Then, the objective functions and the constraints are evaluated analytically using the initial values of design variables and the flowfield solution. The sensitivity information is passed to the optimizer along with the current values of design variables, constraints, and the objective function. The optimizer uses this information to determine a one-dimensional search direction. Along this search direction, the optimizer generates different sets of design variables (i.e., computational grids). In turn, approximate flow analyses are performed to obtain the flowfield solution corresponding to each set of design variables and thereby the objective function and the constraints. This one-dimensional search process continues until the maximum value of the objective function is obtained. At this point, the one-dimensional search process ends and a new optimization iteration starts. Hence, a CFD analysis is performed using the latest design variables and a sensitivity analysis is performed to determine new gradients (new one-dimensional search direction). This algorithm is repeated until an optimum solution is reached. The design algorithm is deemed to have reached an optimum when all the constraints are satisfied, and the objective function has a value, which does not change for a specified number of optimization iterations.

Sensitivity of Optimum Design

After the optimum design is obtained, it is desirable to determine the sensitivity of the optimum design with respect to the problem parameters. Such information is useful to perform trade-off analyses. For example, it may be wished to estimate what effect a specified increase in the freestream Mach number has on the optimum thrust. Mathematically, this requires the derivatives of the optimum values of the objective function and the corresponding design variables with respect to the problem parameters.

The first-order sensitivity derivative method developed in Ref. 13 is adapted for the present study. The vector $\bar{P}$ contains the problem parameters, which are held fixed during the optimization. Using the superscript *op* to denote the optimum quantities, the dependence of F^{op} and $\bar{G}$ on $\bar{X}_D$ and $\bar{P}$ can be written as

$$F^{op} = F^{op}(\bar{Q}(\bar{X}_D^{op}(\bar{P}), \bar{P}), \bar{X}_D^{op}(\bar{P}), \bar{P}) \tag{24}$$

$$\bar{G}_a = \bar{G}_a(\bar{Q}(\bar{X}_D^{op}(\bar{P}), \bar{P}), \bar{X}_D^{op}(\bar{P}), \bar{P}) = 0 \tag{25}$$

where $\bar{G}_a$ is a vector containing only the active constraints at the constrained maximum. A constraint becomes an active one when its value is zero, i.e., the corresponding one of Eqs. (8–10) becomes an equality. The total optimum sensitivity derivative of the objective function with respect to a problem parameter P is obtained using the chain rule of differentiation

$$\frac{dF^{op}}{dP} = \frac{\partial F^{op}}{\partial P} + \left[\left(\frac{\partial F^{op}}{\partial \bar{Q}}\right)^T \frac{\partial \bar{Q}}{\partial \bar{X}_D} + \frac{\partial F^{op}}{\partial \bar{X}_D}\right]^T \frac{\partial \bar{X}_D}{\partial P} + \left(\frac{\partial F^{op}}{\partial \bar{Q}}\right)^T \frac{\partial \bar{Q}}{\partial P} \tag{26}$$

Any perturbation of the parameter P about its value at the initial optimum must be such that the originally active constraints remain active, i.e.,

$$\frac{d\bar{G}_a}{dP} = \frac{\partial \bar{G}_a}{\partial P} + \left[\left(\frac{\partial \bar{G}_a}{\partial \bar{Q}}\right)^T \frac{\partial \bar{Q}}{\partial \bar{X}_D} + \frac{\partial \bar{G}_a}{\partial \bar{X}_D}\right]^T \frac{\partial \bar{X}_D}{\partial P} + \left(\frac{\partial \bar{G}_a}{\partial \bar{Q}}\right)^T \frac{\partial \bar{Q}}{\partial P} = 0 \tag{27}$$

For a constrained optimization problem, the first-order optimality conditions at a local optimum (commonly known as Kuhn-Tucker conditions[14]) are given by Eq. (25) and the following equation:

$$\left[\left(\frac{\partial F^{op}}{\partial \bar{Q}}\right)^T \frac{\partial \bar{Q}}{\partial \bar{X}_D} + \frac{\partial F^{op}}{\partial \bar{X}_D}\right] + \left[\left(\frac{\partial \bar{G}_a}{\partial \bar{Q}}\right)^T \frac{\partial \bar{Q}}{\partial \bar{X}_D} + \frac{\partial \bar{G}_a}{\partial \bar{X}_D}\right]\bar{\psi} = 0 \tag{28}$$

where $\bar{\psi}$ is a vector containing the Langrangian multipliers. Combining Eqs. (27) and (28) yields,

$$\left[\left(\frac{\partial F^{op}}{\partial \bar{Q}}\right)^T \frac{\partial \bar{Q}}{\partial \bar{X}_D} + \frac{\partial F^{op}}{\partial \bar{X}_D}\right]^T \frac{\partial \bar{X}_D}{\partial P} = \bar{\psi}^T \left[\frac{\partial \bar{G}_a}{\partial P} + \left(\frac{\partial \bar{G}_a}{\partial \bar{Q}}\right)^T \frac{\partial \bar{Q}}{\partial P}\right] \tag{29}$$

Equation (29) is put into Eq. (26) in order to eliminate $(\partial \bar{X}_D/\partial P)$,

$$\frac{dF^{op}}{dP} = \frac{\partial F^{op}}{\partial P} + \bar{\psi}^T \frac{\partial \bar{G}_a}{\partial P} + \left[\left(\frac{\partial F^{op}}{\partial \bar{Q}}\right)^T + \bar{\psi}^T \left(\frac{\partial \bar{G}_a}{\partial \bar{Q}}\right)^T\right] \frac{\partial \bar{Q}}{\partial P} \tag{30}$$

The Lagrangian multipliers in Eq. (30) are obtained from the following relation evaluated at the optimum point

$$\bar{\psi} = -\left[\left(\frac{\partial \bar{G}_a}{\partial \bar{X}_D}\right)^T \frac{\partial \bar{G}_a}{\partial \bar{X}_D}\right]^{-1} \left[\frac{\partial \bar{G}_a}{\partial \bar{X}_D}\right]^T \frac{\partial F^{op}}{\partial \bar{X}_D} \tag{31}$$

The derivatives of the conserved variables vector, $\bar{Q}$, with respect to the problem parameters are obtained as follows:

$$\bar{R}(\bar{Q}(\bar{X}_D(\bar{P}), \bar{P}), \bar{X}_D(\bar{P}), \bar{P}) = 0 \tag{32}$$

Differentiation of Eq. (32) with respect to the problem parameters yields

$$\frac{d\bar{R}}{d\bar{P}} = \frac{\partial \bar{R}}{\partial \bar{P}} + \left[\frac{\partial \bar{R}}{\partial \bar{X}_D} + \frac{\partial \bar{R}}{\partial \bar{Q}} \cdot \frac{\partial \bar{Q}}{\partial \bar{X}_D}\right]^T \frac{\partial \bar{X}_D}{\partial \bar{P}} + \frac{\partial \bar{R}}{\partial \bar{Q}} \cdot \frac{\partial \bar{Q}}{\partial \bar{P}} = 0 \tag{33}$$

Using Eq. (14) with Eq. (33) results in

$$\left[\frac{\partial \bar{R}}{\partial \bar{Q}}\right] \frac{\partial \bar{Q}}{\partial \bar{P}} = -\left[\frac{\partial \bar{R}}{\partial \bar{P}}\right] \equiv \bar{R}_v \tag{34}$$

Solving Eq. (34) similar to Eq. (14) for $(\partial \bar{Q}/\partial \bar{P})$ and substituting it into Eq. (30) yields the sensitivities of the objective function to the problem parameters.

Alternatively, the adjoint variable method can be used when the substitution of Eq. (34) into Eq. (30) is performed as follows:

$$\frac{dF^{op}}{dP} = \frac{\partial F^{op}}{\partial P} + \bar{\psi}^T \frac{\partial \bar{G}_a}{\partial P} + \left[\left(\frac{\partial F^{op}}{\partial \bar{Q}}\right)^T + \bar{\psi}^T \left(\frac{\partial \bar{G}_a}{\partial \bar{Q}}\right)^T\right] \cdot J^{-1} \bar{R}_v \tag{35}$$

where $J^{-1} = [\partial \bar{R}/\partial \bar{Q}]^{-1}$. Then, an adjoint vector $\bar{\lambda}$, that satisfies the following equation, is defined

$$J^T \bar{\lambda} = \left[\frac{\partial F^{op}}{\partial \bar{Q}} + \left(\frac{\partial \bar{G}_a}{\partial \bar{Q}} \cdot \bar{\psi}\right)\right] \tag{36}$$

Substitution of Eq. (36) into Eq. (35) gives

$$\frac{dF^{op}}{dP} = \frac{\partial F^{op}}{\partial P} + \bar{\psi}^T \frac{\partial \bar{G}_a}{\partial P} + \bar{\lambda}^T \bar{R}_v \tag{37}$$

The adjoint system of Eq. (36) is independent of any differentiation with respect to the problem parameters. Also, both terms on the right-hand side of Eq. (36) are available from the calculations of Eqs. (11) and (12). The partial derivatives $\partial F^{op}/\partial \bar{P}$, $\partial \bar{G}_a/\partial \bar{P}$ and $\partial \bar{R}/\partial \bar{P}$ can be evaluated analytically. Therefore, the sensitivity derivatives (Eq. 37) are obtained after solving Eq. (36), evaluating Eq. (31), and finally performing the pertinent substitutions.

Since the number of problem parameters $\bar{P}$ (equal to seven for the present example) is greater than the number of the adjoint vectors $\bar{\lambda}$ (equal to one for the present example), the adjoint variable method is more economical[1] for the present example.

Results and Discussion

The present aerodynamic design optimization method is demonstrated by considering the flowfield about a scramjet-

afterbody model (Fig. 2). As indicated earlier, shown in Fig. 2 is the simplified model of the nozzle-afterbody section of a generic hypersonic vehicle (Fig. 1). The upstream flow conditions, which are kept constant during the optimization process are:

1) External Flow: $M_\infty = 6.000$, $T_{0,\infty} = 885°\text{R}$ $P_{0,\infty} = 51{,}984$ psf

2) Internal Flow: $M_{th} = 1.665$, $T_{0,th} = 610°\text{R}$ $P_{0,th} = 3{,}960$ psf

where T_0 and P_0 denote the total temperature and the total pressure, respectively. The throat height of the nozzle H_{th}, is 0.05 ft. All the solid walls are assumed to be impermeable and adiabatic. The dimensions of the computational grid used to analyze the flowfield are 105 × 81 cells (Fig. 3).

Although the flowfield is analyzed using CFD for a range of ramp and cowl angles in the present study, the experimental data[15] are only available for the case with $X_{D1} = 20$ deg and $X_{D2} = 12$ deg. The computed and the measured ramp surface pressure coefficients are compared in Fig. 4. Some discrepancy is observed over the top quarter of the ramp, which may be attributed to the viscous effects that are not represented by the Euler equations of the present study.

To demonstrate the efficiency and the feasibility of the proposed design optimization method, the example problem is solved using three different procedures and the results are given in Table 1. In procedure 1, the sensitivity coefficients [∇F, ∇G_j in Eqs. (11) and (12)] are computed by traditional finite difference method. In procedures 2 and 3, however, they are computed using the quasi-analytical method, i.e., the sensitivity analysis. In procedures 1 and 2, a CFD analysis is performed every time the optimizer changes the design variables. In procedure 3, an approximate flow analysis (Eq. 16) is performed if the optimizer is at the one-dimensional search process, and a CFD analysis is performed when the sensitivity coefficients are needed. The rationale for procedure 3 rests on the fact that the changes in the design variables are much smaller when the one-dimensional search is conducted than their changes when the sensitivity coefficients are computed. All of these procedures are started from the same initial design, where $X_{D1} = 22.9$ deg and $X_{D2} = 17.18$ deg.

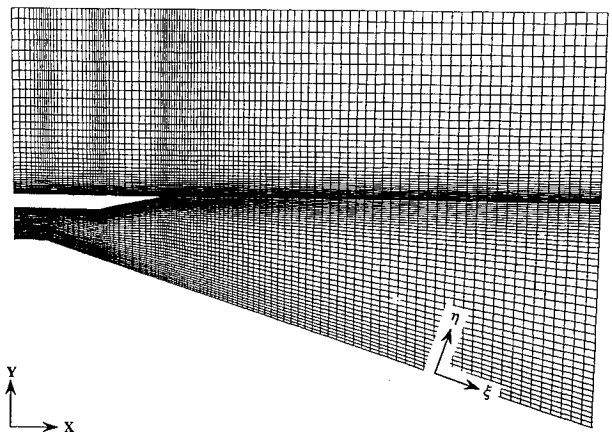

Fig. 3 An example of the computational grid used in the simplified scramjet-afterbody analysis.

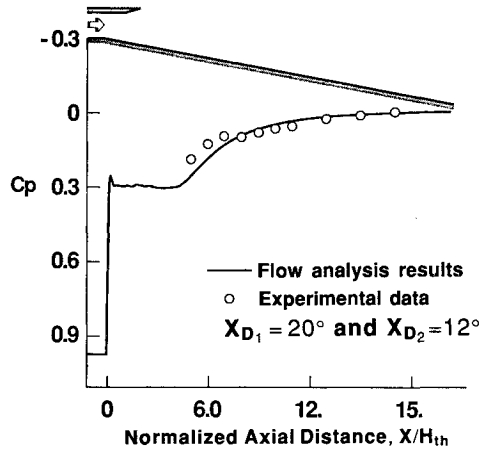

Fig. 4 Comparison of the computed surface pressure coefficients on the ramp with the experimental data.

Since the optimization requires that all constraints be satisfied [Eqs. (8–10)], the values of G_1, G_2, and G_3 are all less than zero. The value of G_1 is closest to zero, which indicates that it is the active constraint for this optimization problem. For the objective and constraint functions as defined by Eqs. (7–10), the optimum ramp and cowl angles are determined to be $X_{D1} = 18.95$ deg and $X_{D2} = 16.62$ deg, respectively. The values of the constants in Eqs. (8–10) used here are $C_1 = 0.6$, $C_2 = 1.0$, $C_3 = 1.5$. The optimum axial thrust values obtained by these procedures differ only by ±0.03%. Therefore, all three procedures have comparable accuracies and they can be considered acceptable for engineering purposes.

In order to assess the relative efficiencies of procedures 1–3, their computational execution times are given in Table 2. Also shown in this table are the number of CFD analyses and the number of approximate flow analyses performed in each procedure. All the execution times are normalized by that of procedure 3, which is approximately 1.39 CPU hour on a single central processing unit (CPU) of the CRAY-2 computer at National Aerodynamic Simulation (NAS) facility of NASA. After a comparison of the execution times, it can easily be concluded that procedure 3 is the most efficient. This is due to the fact that a CFD flow analysis is the most expensive component of the present aerodynamic design optimization method and procedure 3 uses the fewest number of CFD analyses.

All of the present results are obtained using the SIMD (single instruction/multiple data) processing of this four-CPU computer.[16] However, the computational execution times can be reduced significantly by using the MIMD (multiple instruction/multiple data) processing. For example, the CPU time is reduced by 40% and the wall clock time is reduced by 70% when Eq. (14) is solved using the MIMD processing on four CPUs. Most of the total computational speed up,

Table 1 Results of different aerodynamic design optimization procedures

Procedure	X_{D1}, deg	X_{D2}, deg	F	G_1	G_2	G_3
			Initial values			
All	22.91	17.18	0.1201	−0.4223	1.2531	0.4082
			Optimum values			
1	18.34	16.42	0.1319	−0.0156	−0.3812	−0.1234
2	18.85	16.62	0.1322	−0.0162	−0.4030	−0.0685
3	18.95	16.53	0.1325	−0.0124	−0.3586	−0.1008

Table 2 Normalized computational times required by different aerodynamic design optimization procedures

Procedure[a,b]	Execution time	No. of CFD analyses	No. of approx. flow analyses
1	4.480[c]	32	—
2	2.848	20	—
3	1.000	6	14

[a]Grid size (105 × 81).
[b]Number of design variables = 2.
[c]All times are normalized by the time required for procedure 3.

however, should be expected when the CFD analyses are also MIMD processed.

Procedures 1–3 require six optimization iterations (more commonly known as levels) to get a converged optimum solution. The history of the optimization process for procedure 3 is shown in Fig. 5. Shown in Figs. 6 and 7 are the pressure distribution histories on both the ramp and cowl surfaces for different optimization iterations. As expected, the flow expands more rapidly with the increased ramp angle, and that in turn increases the axial thrust force coefficient. However, it should be noted that the ramp angle is bounded by the constraint G_1, which imposes the no-inflow condition at the ramp tip.

Finally, the sensitivities of the optimum axial thrust coefficients with respect to the problem parameters $\bar{P}$, are given in Table 3. In the present demonstrative example, the problem parameters, as mentioned before, are the specific heat ratio γ, Mach numbers, total temperatures, and total pressures of both external and internal flows. Based on the results of Table 3, it can be concluded that the axial thrust force coefficient F, is influenced mainly by γ, M_{th}, $P_{0,th}$ and $P_{0,\infty}$. Accuracies of the sensitivity derivatives are verified by solving perturbed optimization problems for each design parameter P, i.e., via the finite difference approximation. However, verifying the influence of γ on F with the finite difference method cannot be done using the present CFD analysis method, which is for constant γ flows.

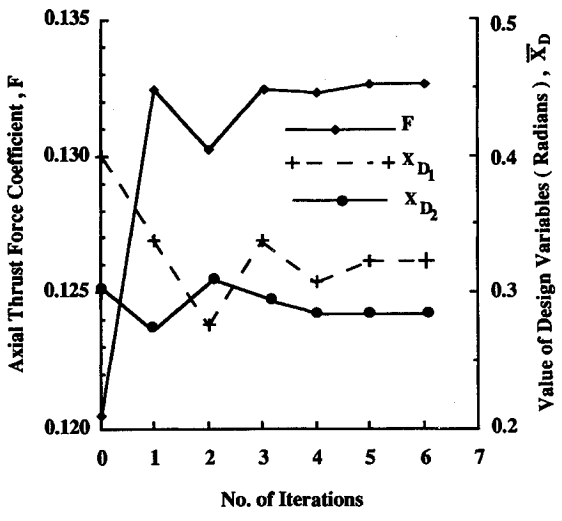

Fig. 5 History of the optimization process.

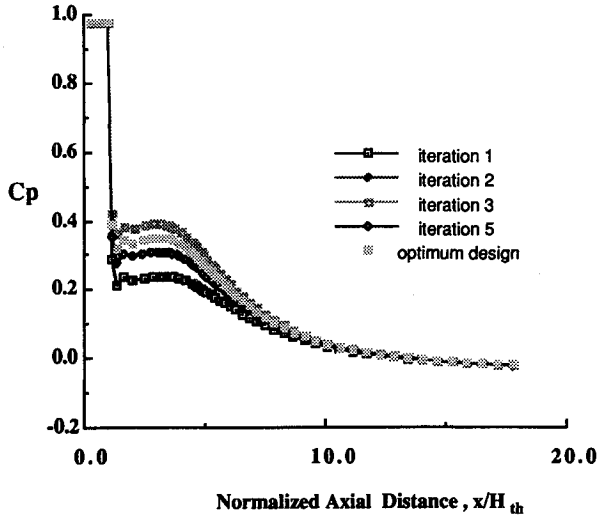

Fig. 6 Variation of the ramp surface pressure coefficients with the optimization iterations.

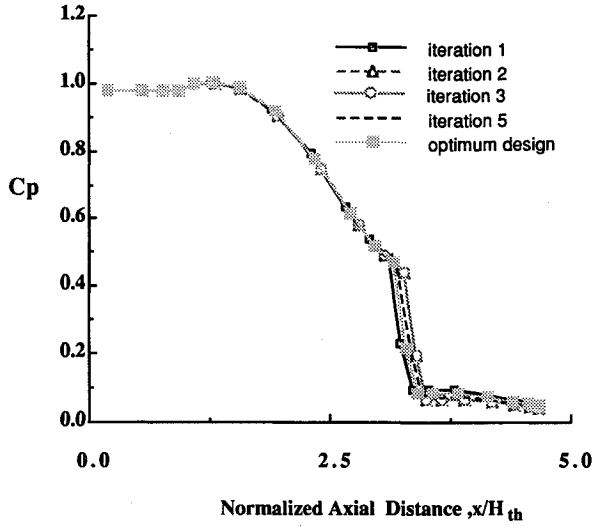

Fig. 7 Variations of the cowl surface pressure coefficients with the optimization iterations.

Table 3 Values of the sensitivity derivatives for the optimum axial thrust coefficient using different approaches

Sensitivity derivative	Sensitivity analysis approach[a]	Finite difference approach
$\frac{dF/F}{dM_\infty/M_\infty}$	$-1.10*10^{-5b}$	$-1.00*10^{-5}$
$\frac{dF/F}{dP_{0,\infty}/P_{0,\infty}}$	$-2.05*10^{-1}$	$-2.05*10^{-1}$
$\frac{dF/F}{dT_{0,\infty}/T_{0,\infty}}$	$-1.85*10^{-4}$	$-1.94*10^{-4}$
$\frac{dF/F}{dM_{th}/M_{th}}$	$-2.63*10^{-1}$	$-2.63*10^{-1}$
$\frac{dF/F}{dP_{0,th}/P_{0,th}}$	$-3.62*10^{-2}$	$-3.63*10^{-2}$
$\frac{dF/F}{dT_{0,th}/T_{0,th}}$	$-1.82*10^{-3}$	$-1.85*10^{-3}$
$\frac{dF/F}{d\gamma/\gamma}$	$-8.64*10^{-1}$	—

[a]Results are based on the values of $\bar{X}_D$ at the optimum design point.
[b]All results are normalized by the values of F and problem parameters at the optimum design point.

Conclusions

An efficient aerodynamic design optimization method is developed. The method consists of CFD flow analyses, quasi-analytical evaluations of all required gradients by means of sensitivity analyses, approximate flow analyses, and an optimization algorithm. This procedure is successfully applied to a scramjet-afterbody configuration for an optimum axial thrust force coefficient.

Three different design optimization procedures are presented to demonstrate the feasibility and the accuracy. Comparisons between these procedures indicate that all of these procedures yield results with very small differences. However, the procedure, which employs the quasi-analytical approach and requires the fewest CFD analyses, is the most economical one.

The sensitivity of the optimum axial thrust coefficient to the variations in the problem parameters is obtained by the

quasi-analytical approach as well as the finite difference approach. This sensitivity information indicates that the specific heat ratio, the internal Mach number, and the external and the internal total pressures are the most influential problem parameters.

The present method can easily be used for a shape optimization, where the number of design variables is much larger than that of the present demonstrative example. Moreover, the existence of discontinuities, such as shocks, and other nonlinearity sources may necessitate higher order approximations to the fluid dynamics equations. An extension of the present investigation,[17] therefore, has reported on the shape optimization of the current scramjet-afterbody example using an up to third-order approximation of the Euler equations. Furthermore, the sensitivity analysis for the Navier-Stokes equations have also been developed recently and applied to optimize the shape of a transonic airfoil.

Acknowledgments

The research work is supported by NASA Langley Research Center under Grant NAG-1-1188. David S. Miller is the technical monitor.

References

[1]Baysal, O., and Eleshaky, M. E., "Aerodynamic Sensitivity Analysis Methods for the Compressible Euler Equations," *Recent Advances and Applications in CFD*, edited by O. Baysal, ASME-FED, Vol. 103, Winter Annual Meeting, Nov. 1990, pp. 191–202. Also, *ASME Journal of Fluids Engineering*, Vol. 113, No. 4, Dec. 1991.

[2]Elbanna, H., and Carlson, L., "Determination of Aerodynamic Sensitivity Coefficients in the Transonic and Supersonic Regimes," AIAA Paper 89-0532, Jan. 1989.

[3]Rao, G. V. R., "Exhaust Nozzle Contour for Optimum Thrust," *Jet Propulsion*, Vol. 38, No. 6, 1958, pp. 377-382.

[4]Nickerson, G. R., Dunn, S. S., and Migdal, D., "Optimized Supersonic Exhaust Nozzles for Hypersonic Propulsion," AIAA Paper 88-3161, 1988.

[5]Doty, J. H., Thompson, H. D., and Hoffman, J. D., "Optimum Thrust Two-Dimensional NASP Nozzle Study," NASP CR-1069, NASA Langley Research Center, Hampton, VA, 1989.

[6]Baysal, O., Engelund, W. C., Eleshaky, M. E., and Pittman, J. L., "Adaptive Computations of Multispecies Mixing Between Scramjet Nozzle Flows and Hypersonic Freestream," AIAA Paper 89-0009, Jan. 1989. Also, *Journal of Propulsion and Power*, Vol. 8, No. 1, 1992.

[7]Vanderplaats, G. N., "An Efficient Feasible Direction Algorithm for Design Synthesis," *AIAA Journal*, Vol. 22, No. 11, 1984, pp. 1633–1640.

[8]Anderson, W. K., Thomas, J. L., and Van Leer B., "Comparison of Finite Volume Flux Vector Splittings for the Euler Equations," *AIAA Journal*, Vol. 24, No. 9, 1986, pp. 1453–1460.

[9]Hansen, S. R., and Vanderplaats, G. N., "Approximation Method for Configuration Optimization of Trusses," *AIAA Journal*, Vol. 28, No. 1, 1990, pp. 161–168.

[10]Martin, R. S., and Wilkinson, J. H., "Solution of Symmetric and Unsymmetric Band Equations and the Calculation of Eigenvectors of Band Matrices," *Numerische Mathematik*, Bd. 9, 1967, pp. 279–301.

[11]Baysal, O., Fouladi, K., and Lessard, V., "A Multigrid and Upwind Viscous Flow Solver on 3-D Overlapped/Embedded Grid," *AIAA Journal*, Vol. 29, No. 6, 1991, pp. 903–910.

[12]Vanderplaats, G. N., "ADS—A Fortran Program for Automated Design Synthesis," NASA CR-177985, Sept. 1985.

[13]Sobieski, J. S., and Barthelemy, J. M., "Optimum Sensitivity Derivatives of Objective Functions in Nonlinar Programming," *AIAA Journal*, Vol. 21, No. 6, 1983, pp. 913–915.

[14]Reklaitis, G. V., Ravindran, A., and Ragsdell, K. M., *Engineering Optimization Methods and Applications*, 1st ed., Wiley, New York, 1983, pp. 191–203.

[15]Cubbage, J. M., and Monta, W. J., "Surface Pressure Data on a Scramjet External Nozzle Model at Mach 6 Using a Simulant Gas for the Engine Flow Exhaust," NASP CR-1058, Feb. 1990.

[16]Baysal, O., "Supercomputing of Supersonic Flows Using Upwind Relaxation MacCormack Schemes," *ASME Journal of Fluids of Engineering*, Vol. 110, No. 1, 1988, p. 62–68.

[17]Baysal, O., Eleshaky, M. E., and Burgreen, G. W., "Aerodynamic Shape Optimization Using Sensitivity Analysis on Third-Order Euler Equations," AIAA Paper 91-1577 CP, *Proceedings of 10th Computational Fluid Dynamic Conference*, June 1991.

[18]Eleshaky, M. E., Baysal, O., "Airfoil Shape Optimization Using Sensitivity Analysis on Viscous Flow Equations," *Multidisciplinary Applications of CFD*," edited by O. Baysal, ASME-FED, Vol. 119, Winter Annual Meeting, Dec. 1991, pp. 26–36.